

Extreme ultraviolet proximity lithography for fast, flexible and parallel fabrication of infrared antennas

Georg Kunkemöller,^{1,2,3} Tobias W. W. Maß,⁴ Ann-Katrin U. Michel,⁴ Hyun-Su Kim,² Sascha Brose,¹ Serhiy Danylyuk,¹ Thomas Taubner,⁴ and Larissa Juschkin^{2,3,*}

¹Chair for the Technology of Optical Systems, RWTH Aachen University and JARA – Fundamentals of Future Information Technology (JARA-FIT), Steinbachstr. 15, 52074 Aachen, Germany

²Chair for the Experimental Physics of EUV, RWTH Aachen University, JARA-FIT, 52074 Aachen, Germany

³Peter Grünberg Institut (PGI-9), Forschungszentrum Jülich GmbH, JARA-FIT, 52425 Jülich, Germany

⁴Institute of Physics (IA), RWTH Aachen University, 52056 Aachen, Germany

*larissa.juschkin@rwth-aachen.de

Abstract: We present a method for fabrication of large arrays of nano-antennas using extreme-ultraviolet (EUV) illumination. A discharge-produced plasma source generating EUV radiation around 10.88 nm wavelength is used for the illumination of a photoresist via a mask in a proximity printing setup. The method of metallic nanoantennas fabrication utilizes a bilayer photoresist and employs a lift-off process. The impact of Fresnel-diffraction of EUV light in the mask on a shape of the nanostructures has been investigated. It is shown how by the use of the same rectangular apertures in the transmission mask, antennas of various shapes can be fabricated. Using Fourier transform infrared spectroscopy, spectra of antennas reflectivity were measured and compared to FDTD simulations demonstrating good agreement.

©2015 Optical Society of America

OCIS codes: (220.3740) Lithography; (300.6340) Spectroscopy, infrared.

References and links

1. Z. Fang and X. Zhu, "Plasmonics in Nanostructures," *Adv. Mater.* **25**(28), 3840–3856 (2013).
2. S. Zeng, D. Baillargeat, H.-P. Ho, and K.-T. Yong, "Nanomaterials enhanced surface plasmon resonance for biological and chemical sensing applications," *Chem. Soc. Rev.* **43**(10), 3426–3452 (2014).
3. S. Law, V. Podolskiy, and D. Wasserman, "Towards nano-scale photonics with micro-scale photons: the opportunities and challenges of mid-infrared plasmonics," *Nanophotonics* **2**(2), 103–130 (2013).
4. R. F. Aroca, "Surface-Enhanced Vibrational Spectroscopy," Wiley (2006).
5. Y. Chen and H. Ming, "Review of surface plasmon resonance and localized surface plasmon resonance sensor," *Photonic Sens.* **2**(1), 37–49 (2012).
6. K. A. Willets and R. P. Van Duyne, "Localized Surface Plasmon Resonance Spectroscopy and Sensing," *Annu. Rev. Phys. Chem.* **58**(1), 267–297 (2007).
7. H. A. Atwater and A. Polman, "Plasmonics for improved photovoltaic devices," *Nat. Mater.* **9**(3), 205–213 (2010).
8. Z. Li, M. Mutlu, and E. Ozbay, "Chiral metamaterials: from optical activity and negative refractive index to asymmetric transmission," *J. Opt.* **15**(2), 023001 (2013).
9. T. G. Mackay, "Negatively refracting chiral metamaterials: a review," *J. Photonics Energy* **1**, 018003 (2010).
10. C. Ayala-Orozco, C. Urban, S. Bishnoi, A. Urban, H. Charron, T. Mitchell, M. Shea, S. Nanda, R. Schiff, N. Halas, and A. Joshi, "Sub-100nm gold nanomatryoshkas improve photo-thermal therapy efficacy in large and highly aggressive triple negative breast tumors," *J. Control. Release* **191**, 90–97 (2014).
11. S. Lal, N. K. Grady, J. Kundu, C. S. Levin, J. B. Lassiter, and N. J. Halas, "Tailoring plasmonic substrates for surface enhanced spectroscopies," *Chem. Soc. Rev.* **37**(5), 898–911 (2008).
12. S. Schlücker, "Surface-Enhanced Raman Spectroscopy: Concepts and Chemical Applications," *Angew. Chem. Int. Ed. Engl.* **53**(19), 4756–4795 (2014).
13. G. R. Brewer, "Electron-beam technology in microelectronic fabrication," Academic Press: New York, (1980).
14. J. Melngailis, "Focused Ion-Beam Technology and Applications," *J. Vac. Sci. Technol. B* **5**(2), 469–495 (1987).
15. J. Zhao, B. Frank, S. Burger, and H. Giessen, "Large-area high-quality plasmonic oligomers fabricated by angle-controlled colloidal nanolithography," *ACS Nano* **5**(11), 9009–9016 (2011).

16. J. M. Hoffmann, X. Yin, J. Richter, A. Hartung, T. W. W. Maß, and T. Taubner, "Low-Cost Infrared Resonant Structures for Surface-Enhanced Infrared Absorption Spectroscopy in the Fingerprint Region from 3 to 13 μm ," *J. Phys. Chem. C* **117**(21), 11311–11316 (2013).
17. Y.-C. Chang, S.-C. Lu, H.-C. Chung, S.-M. Wang, T.-D. Tsai, and T.-F. Guo, "High-Throughput Nanofabrication of Infrared and Chiral Metamaterials using Nanospherical-Lens Lithography," *Sci. Rep.* **3**, 3339 (2013).
18. S. Cataldo, J. Zhao, F. Neubrech, B. Frank, C. Zhang, P. V. Braun, and H. Giessen, "Hole-Mask Colloidal Nanolithography for Large-Area Low-Cost Metamaterials and Antenna-Assisted Surface-Enhanced Infrared Absorption Substrates," *ACS Nano* **6**(1), 979–985 (2012).
19. S. Aksu, A. A. Yanik, R. Adato, A. Artar, M. Huang, and H. Altug, "High-Throughput Nanofabrication of Infrared Plasmonic Nanoantenna Arrays for Vibrational Nanospectroscopy," *Nano Lett.* **10**(7), 2511–2518 (2010).
20. A. A. Yanik, A. E. Cetin, M. Huang, A. Artar, S. H. Mousavi, A. Khanikaev, J. H. Connor, G. Shvets, and H. Altug, "Seeing protein monolayers with naked eye through plasmonic Fano resonances," *Proc. Natl. Acad. Sci. U.S.A.* **108**(29), 11784–11789 (2011).
21. S. Bagheri, H. Giessen, and F. Neubrech, "Large-Area Antenna-Assisted SEIRA Substrates by Laser Interference Lithography," *Adv. Opt. Mater.* **2**(11), 1050–1056 (2014).
22. K. Chen, R. Adato, and H. Altug, "Dual-Band Perfect Absorber for Multispectral Plasmon-Enhanced Infrared Spectroscopy," *ACS Nano* **6**(9), 7998–8006 (2012).
23. S. Bagheri, K. Weber, T. Gissibl, T. Weiss, F. Neubrech, and H. Giessen, "Fabrication of Square-Centimeter Plasmonic Nanoantenna Arrays by Femtosecond Direct Laser Writing Lithography: Effects of Collective Excitations on SEIRA Enhancement," *ACS Photonics* **2**(6), 779–786 (2015).
24. S. Danylyuk, H. Kim, S. Brose, C. Dittberner, P. Loosen, T. Taubner, K. Bergmann, and L. Juschkin, "Diffraction-assisted extreme ultraviolet proximity lithography for fabrication of nanophotonic arrays," *J. Vac. Sci. Technol. B* **31**(2), 021602 (2013).
25. J. Pankert, K. Bergmann, R. Wester, J. Klein, W. Neff, O. Rosier, S. Seiwert, S. Smith, S. Probst, D. Vaudrevange, G. Siemons, J. Apetz, J. Jonkers, M. Loeken, T. Krücken, and P. Zink, "Hollow-Cathode-Triggered Plasma Pinch Discharge," in *EUV Sources for Lithography*, V. Bakshi, ed. (SPIE press, 2005).
26. K. Bergmann, O. Rosier, W. Neff, and R. Lebert, "Pinch-Plasma Radiation Source for Extreme-Ultraviolet Lithography with a Kilohertz Repetition Frequency," *Appl. Opt.* **39**(22), 3833–3837 (2000).
27. K. Bergmann, S. V. Danylyuk, and L. Juschkin, "Optimization of a gas discharge plasma source for extreme ultraviolet interference lithography at a wavelength of 11 nm," *J. Appl. Phys.* **106**(7), 073309 (2009).
28. S. Brose, S. Danylyuk, L. Juschkin, C. Dittberner, K. Bergmann, J. Moers, G. Panaitov, S. Trellenkamp, P. Loosen, and D. Grützmacher, "Broadband transmission masks, gratings and filters for extreme ultraviolet and soft X-ray lithography," *Thin Solid Films* **520**(15), 5080–5085 (2012).
29. Allresist GmbH, Product Datasheets, <http://www.allresist.de/produkte/>.
30. B. Meliorisz, "Simulation of mask proximity printing," *J. Micro/Nanolith, MEMS MOEMS* **6**(2), 023006 (2007).
31. T. Fühner, T. Schnattinger, G. Ardelean, and A. Erdmann, "Dr. Litho - a development and research lithography simulator," *Proc. SPIE* **6520**, 65203F (2007).
32. F. Neubrech, D. Weber, D. Enders, T. Nagao, and A. Pucci, "Antenna Sensing of Surface Phonon Polaritons," *J. Phys. Chem. C* **114**(16), 7299–7301 (2010).
33. J. M. Hoffmann, H. Janssen, D. N. Chigrin, and T. Taubner, "Enhanced infrared spectroscopy using small-gap antennas prepared with two-step evaporation nanosphere lithography," *Opt. Express* **22**(12), 14425–14432 (2014).
34. C. D'Andrea, J. Bochterle, A. Toma, C. Huck, F. Neubrech, E. Messina, B. Fazio, O. M. Maragò, E. Di Fabrizio, M. Lamy de La Chapelle, P. G. Gucciardi, and A. Pucci, "Optical nanoantennas for multiband surface-enhanced infrared and raman spectroscopy," *ACS Nano* **7**(4), 3522–3531 (2013).
35. V. Liberman, R. Adato, A. Mertiri, A. A. Yanik, K. Chen, T. H. Jeys, S. Erramilli, and H. Altug, "Angle-and polarization-dependent collective excitation of plasmonic nanoarrays for surface enhanced infrared spectroscopy," *Opt. Express* **19**(12), 11202–11212 (2011).

1. Introduction

Plasmonics with nanostructures has been studied extensively during the last decades [1–3]. The ability of nanostructures to confine light and enable its control on a subwavelength scale led to a variety of applications like Surface Enhanced Spectroscopy [4], plasmonic sensors [5,6], solar cells [7], chiral metamaterials [8,9] and medical applications like cancer therapy [10]. Tailoring the optical properties of metallic nano- or micro- structures in order to achieve a high local field enhancement at a desired illumination wavelength is beneficial for e.g. molecular sensing in surface enhanced Raman-Spectroscopy (SERS) and surface enhanced infrared absorption (SEIRA) spectroscopy [11,12]. Thus, the progress in these fields relies on the availability of suited fabrication methods, which offer precise shape and size control, high throughput and low costs. Common methods for the fabrication of nano- and microstructures are Electron-Beam (EBL) [13] and Focused Ion Beam (FIB) lithography [14], which offer a

high flexibility for the design of structure geometries and patterns at a high resolution of a few tens of nanometers. However, both EBL and FIB suffer from a slow serial writing process and thus have a relatively low throughput and comparably high costs.

Recently, several lithographic approaches to improve throughput and to lower costs by using parallel fabrication processes were introduced. Nanosphere Lithography (NSL) can use self assembled nano- [15] and micrometer-sized [16] spheres as a shadow-mask for metal evaporation and the fabrication of hexagonally arranged antennas. Nanospherical-lens Lithography uses self-assembled polystyrene beads to focus UV-light and create large-area, sub 100 nm Au nanodisc arrays [17]. Hole-Mask Colloidal Nanolithography uses immobilized, well separated polystyrene spheres to create a mask for tilted-angle evaporation and the large-area fabrication of various split ring structures [18]. A disadvantage of methods using nano- or microspheres as evaporation mask is a limited control over the self-assembly of the spheres and thus insufficient flexibility in pattern design. Lift-off free evaporation methods, e.g. Nanostencil-Lithography, make use of EBL to create a reusable mask for metal evaporation [19,20]. Hereby, a change of structure geometry requires the fabrication of a new mask using serial lithography methods.

These recently developed methods seek to circumvent a serial fabrication process at a cost of flexibility in structure or pattern design. In contrast to that, the recent approach of Laser Interference Lithography is a promising method, which offers the large-area, fast and flexible fabrication of metallic antennas with resonances in the near- and mid-IR spectral range [21]. Though, with this method, no single structures can be fabricated and for more complicated structure geometries and thus for different applications and desired properties such as e.g. multi-band SEIRA [22] and chirality [8], this fabrication method has yet to prove its capabilities. Also recently, the possibility to fabricate large arrays of linear antennas by using direct laser writing has been shown [23]. Although this method belongs to the serial fabrication techniques, it might, besides the limited resolution, also enable a fast and flexible fabrication of nearly arbitrary shaped infrared antennas over several mm².

As an alternative method, we present Extreme Ultraviolet (EUV) Proximity Lithography as a fabrication technique that offers a fast, flexible and parallel fabrication of many microstructures suited for SEIRA. In contrast to standard UV lithography, a patterning of a variety of structures by using only a single transmission mask is possible. In a previous publication [24], we already demonstrated how Fresnel diffraction could affect the exposure results. Exemplary patterned photoresists revealed complex structure geometries that are predicted by simulations. Now, we adapt a process for transferring the positive tone photoresist pattern of several complex structures into a suitable antenna material. Finally, selected arrays of antennas are characterized via FTIR reflectance measurements. The obtained experimental results are compared to simulations. With this we demonstrate the feasibility of this new fabrication technique to enable the fabrication of complex structure geometries, small feature-sizes and the fast processing of large substrate areas. Also different substrate materials may be employed in this method.

2. EUV proximity lithography

2.1 Fabrication technology

The principle of operation of the presented lithography tool is depicted in Fig. 1. EUV-radiation emitted by a gas-discharge source and collimated by a pinhole illuminates a transmission mask. The photoresist-coated wafer is brought into close proximity to the mask to enable proximity printing of the photoresist. The mask is attached to a precise-motion holder for controlling mask-wafer alignment and positioning. The entire setup is placed inside a vacuum chamber to avoid absorption of EUV radiation by ambient atmosphere. At the edges of the mask holder, three capacitive proximity sensors are installed for monitoring of the distance between mask and wafer also called the proximity gap.

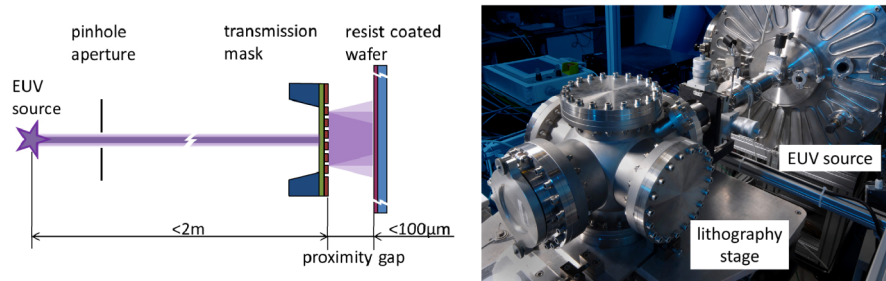


Fig. 1. Schematics and photograph of the lithography tool used for illumination. The EUV source operates at a wavelength of 10.88 nm, illuminating the photoresist through a mask containing the antenna design. The proximity gap can be tuned in the range of few micrometers to several tens of micrometers.

The gas discharge-produced plasma source was developed at the Fraunhofer Institute for Laser Technology and is described in [25,26]. EUV radiation in such type of sources is produced by spectral line emission from highly ionized atoms of the discharge carrier, such as Xe, Ar and other gases. By using gas mixtures of Xe and Ar, along with appropriate band-pass spectral filtering, the spectrum with maximum emission at 10.88 nm with a bandwidth of 3.4% is obtained [27].

The transmission mask technology has been reported before in [28]. The mask consists of a combination of a 100-nm-thick EUV transmissive Nb layer and a 60-nm-thick strongly opaque Ni layer serving as the absorber. This absorbing layer is structured according to the design of the antennas. The mask area, manufactured by this technology, can be as large as $2 \times 2 \text{ mm}^2$, enabling parallel structuring of nanoarrays. The wafer is spring-loaded onto the holding frame and positioned in the mask's close proximity. By using the proximity sensor signal, the wafer and the mask planes can be aligned with respect to each other. The smallest proximity gap is usually of a few micrometers due to technical limitations like unevenness of mask or wafer or imperfect planar alignment between them. The pattern printed into the resist is thus modified by near-field diffraction. The diffraction pattern produced by the mask structures has been simulated and compared to exposure results in photoresist [24]. It was suggested that the diffraction pattern could enable the fabrication of different structures with the same mask by varying parameters such as exposure, distance and period of the structures. Here we report on the fabrication and characterization of such structures. Also a functionality of the antenna arrays was demonstrated using FTIR spectroscopy.

2.2 The bilayer technique

After resist structuring, the pattern has to be transferred into a suitable antenna material such as gold. We used a lift-off process, which has the advantage that it is applicable to any antenna material since the photoresist is patterned on the bare substrate and the functional layer is subsequently deposited.

Lift-off fabrication requires the sidewalls of the structured resist being negatively sloped, i.e. features must be broader at the bottom than at the top. Since the strong absorption of EUV radiation in matter causes the dose reaching deeper regions of the resist layer to be smaller, the developed features are narrower at the bottom than at the top for positive resists. This problem was addressed by using a stack of different resists. In the bilayer scheme, the bottom layer consists of a resist that has a higher sensitivity than the resist used for the top layer. This means it requires a smaller dose than the layer above, so it will develop a wider pattern at the same dose. If the resist layers are thin enough the dose reduction through absorption can be compensated through the higher sensitivity. Accordingly, we used a well-established stack of PMMA resists [29] and adapted the layer thicknesses to be as thin as possible. It is necessary to keep in mind that the thickness of material deposited after resist structuring should not have more than half the thickness of the lower resist layer.

First the bottom resist, a PMMA/MA copolymer (AR-P 617 [29]) with a solid fraction of 1,5%, is deposited by spin-coating at 6000 rpm onto a 2"-silicon wafer. This is followed by a 10 minutes bake on a hotplate at 200°C. Then the upper layer, the PMMA resist (AR-P 679 PMMA 950K [29]) with a solid fraction of 1%, is spun onto the wafer also at 6000 rpm. Then the wafer is put onto the hotplate for another 5 minutes at 180°C. The wafer is then illuminated and subsequently developed in a mixture of MIBK:IPA = 1:3 (AR-P 600-55 [29]) for 1 min. Development is stopped by immersing the wafer for 30 s in IPA and cleaning it in a DI-water bath. A few nanometer thick adhesion layer of Cr and subsequently a layer of Au are evaporated onto the wafer (Leybold L560 Physical Vapor Deposition System). The total metal thickness was determined to be 26.3 nm by AFM measurements. Lifting off the photoresist is done with a remover, which is especially suited for metallized resists (AR 300-70 [29]). The remover is heated to 60°C and with mild ultrasound agitation the resist layer can be fully removed without lifting off the antennas themselves. The wafer is finally cleaned with IPA and DI-water.

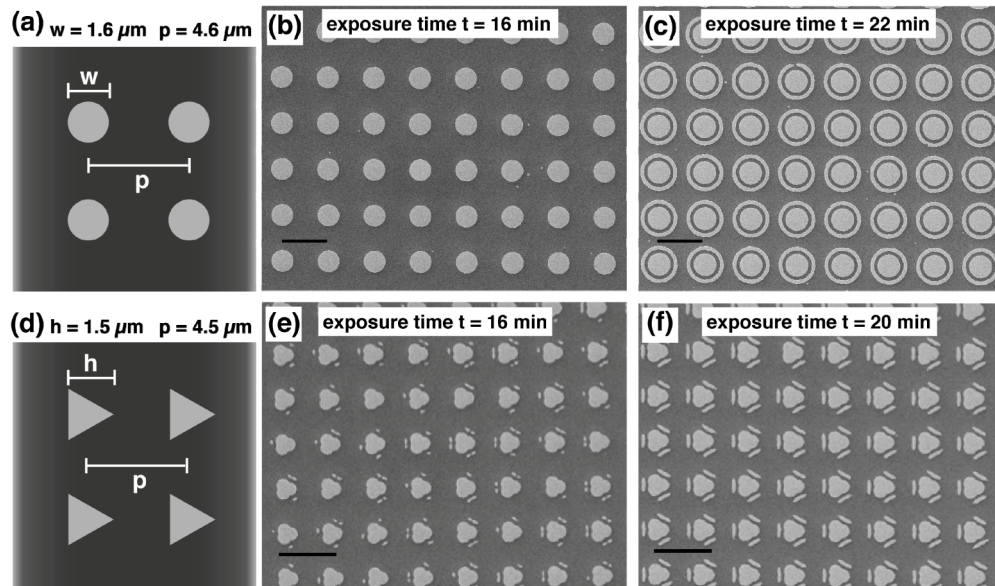


Fig. 2. Structure formation using circular and equilateral triangular apertures: In (a) and (d), schematics of the mask with diameter or length and period of the apertures is shown. In (b) and (c), SEM images of the wafer structures emerging from circular apertures with 16 min and 22 min exposure time, respectively. In (e) and (f), SEM images of the structures emerging from equilateral triangular apertures with 16 min and 20 min exposure time, respectively. All scale bars correspond to a length of 5 μm .

3. Results

3.1 Fabrication

We applied EUV lithography as described above using a single transmission mask with different aperture patterns in order to fabricate arrays of complex metallic structures. Varying the exposure times we manage to fabricate significantly different structure geometries that can substantially modify optical properties. First column in the Fig. 2 shows the patterns of the used transmission mask with arrays of (a) circular and (d) triangular apertures. The SEM images of resulting metallic structures in Fig. 2(b) and 2(c) correspond to the aperture geometry given in (a) and differ in the exposure time, which is 16 min and 22 min, respectively. With the increased exposure time in (c), the dot structures that can be seen in (b) become larger and a secondary fringe of the Fresnel interference pattern becomes visible as an additional outer ring. Similarly, the SEM images in (e) and (f) correspond to the triangular

aperture geometry given in (d) and exposure times of 16 min and 20 min, respectively. For exposure times lower than indicated in the figures, only the inner structure from figures (b) and (e) was observed without secondary structures. For the chosen exposure time, the finer structures in (b) resulting from higher order Fresnel diffraction are either not transferred into the resist or fully removed during liftoff, while in (e) they are partially present. For 20 min EUV exposures, the smaller structures can be successfully converted into metallic structures with a high homogeneity. Examples in Fig. 2 underline the potential of EUV lithography for a high flexibility in fabrication of high quality metallic structures.

In the following investigations we focused on structures fabricated with 230 nm wide rod-shaped apertures. A schematic of the used mask is shown in Fig. 3(a) with indicated parameters. As described in the previous publication [24], we simulate the aerial image behind the mask aperture with the Dr. Fresnel software package for contact and proximity printing (part of the Dr. Litho tool for lithography simulation [30,31]). In Fig. 3(b) and 3(c) the simulated intensity distributions of two different aperture arrays are shown. Since the actual distance between the mask and the sample surface is not exactly known, the proximity gaps were chosen so that a good match with regard to the shape of the antenna can be found. We have to note that the simulation relies on several assumptions and approximations. For example, the illumination spectrum in experiments may deviate from that used in simulations. Also the simulation model uses the Rayleigh-Sommerfeld diffraction integral of the first type (RSI) and therefore approximates the mask as a two-dimensional binary aperture. Since the mask is around 160 nm thick, i.e. several wavelengths scale, and also features some uneven surface topography, these may result in differences between simulation and experimental results. Nevertheless, we find a good agreement between shapes of the simulated structures and the electron microscope images of the fabricated nanoantennas (Fig. 3(d)-3(f)) that were created by EUV exposures. The SEM images in Fig (d) and (e) show antennas that result from the same array. A difference between them is the illumination time: the case shown in (e) was exposed 2 minutes longer compared to (d). In the simulations that are shown as insets in the corresponding SEM images, this is realized by different threshold values imposed to the intensity distributions. For longer illumination time in (e), the threshold intensity value was decreased compared to that in (d). The shapes of fabricated antennas and those in the simulations agree fairly well. This is also the case in Fig. 3(f), where a slightly different aperture geometry and period of the mask pattern is used.

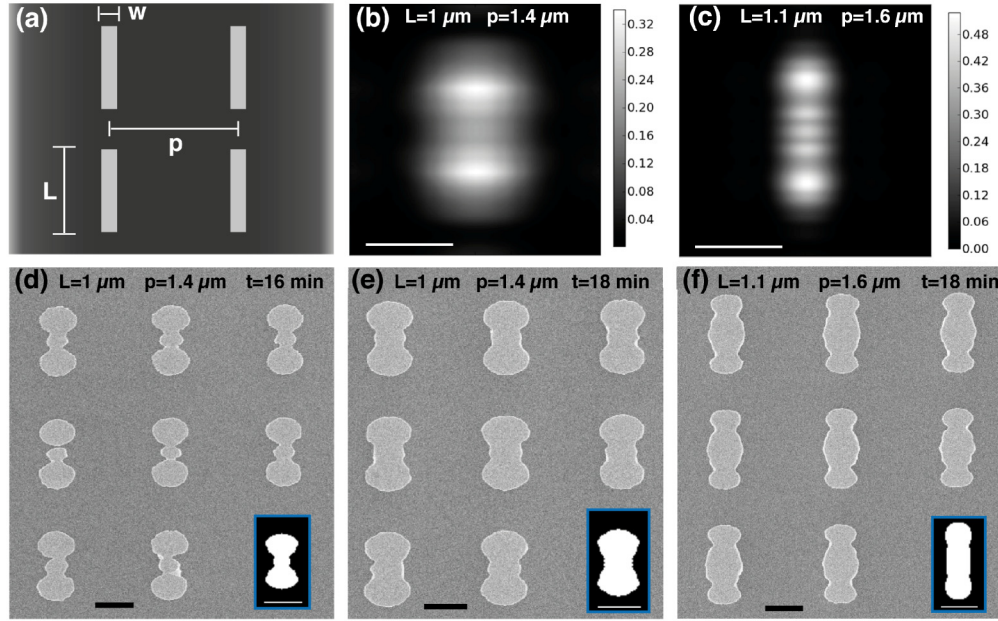


Fig. 3. Structure formation using rod-shaped apertures: In (a), a schematic of the mask with length, width and period of the rectangular apertures is shown. The width of the apertures is $0.23 \mu\text{m}$ and the length, period and illumination time varies as indicated. Simulated intensity distributions are shown in (b) with $10 \mu\text{m}$ and in (c) with $6 \mu\text{m}$ distance to the aperture plane, respectively. In (d) - (f), SEM images of the metallic structures are presented. The insets show the results of the thresholded simulations. (b) corresponds to (d) and (e) with different thresholds and (c) corresponds to (f). All scale bars correspond to a length of 500 nm .

3.2 Measurements of spectral reflectivity of the antenna arrays

The fabricated structures have been characterized by FTIR. The reflection measurements of the different antenna arrays are performed in the mid-IR spectral range using a *Bruker Vertex 70* spectrometer and a *Hyperion 2000* microscope using a knife-edge aperture with the size of $50 \times 50 \mu\text{m}^2$ and a $36\times$ objective. A polarizer is used to decompose the response of the long and the short axis, respectively. All reflection spectra are normalized to the reflection of the bare substrate next to the antenna arrays. The experimentally obtained spectra are shown in Fig. 4(a)-4(c). The main resonances related to the excitation of dipole-like charge carrier oscillations along the long axis of the three structures occur for wavelengths in the range of $5\text{--}8 \mu\text{m}$ (red curves). Water absorption lines between 6 and $7 \mu\text{m}$ cause the spectra to be slightly noisy. Additionally, the excitation of the surface phonon polaritons at the native silicon oxide layer causes a distorted lineshape around $8 \mu\text{m}$ [32,33]. At one third of the fundamental resonance wavelength, i.e. at around $2 \mu\text{m}$, a higher order mode can be observed. Aligning the polarization direction along the short axis of the antennas leads to a resonance between 2 and $4 \mu\text{m}$, which can be attributed to resonant dipole-like excitations of charge carrier oscillations in the ellipsoidal ends of the structures (black dashed curves). The different resonance positions for the two polarization directions turn the structures to be suited for multi-band enhanced spectroscopy [23,34]. Especially advantageous is the fact that the geometry and, thus, the resonance positions of the structures can easily be altered by a change of the exposure time without changing the mask.

The resonances for both long and short axis are well reproduced by the FDTD calculations in Fig. 4(d)-4(f). These calculations are made with “Lumerical” software package, a commercially available FDTD solver. In the simulations, the antenna arrays are simulated with a unit cell consisting of 25 nm thick Au antenna (the thin Cr layer is neglected) with periodic boundaries. The structure dimensions are based on mean values obtained from SEM

images shown in Fig. 3(a)-3(c). The silicon substrate is modeled as dielectric material with a constant refractive index of 3.4. A Drude model was used to model the dielectric data of gold in this spectral range. The overall mesh grid was defined as 25 mesh cells per wavelength. Subgridding methods are used to refine locally the mesh cells down to 2 nm. Acceptable convergence is ensured by defining an auto shutoff level of 10^{-3} for the E-field decay in the simulation region [35]. Linearly polarized collimated light is normally incident onto the antenna arrays in order to obtain a broadband spectrum in a single simulation run. During the measurements, however, the light is focused with a 36x Schwarzschild-objective (NA = 0.5) that causes incident angles ranging from 10° - 30° . Differences between measurement and simulation can be seen e.g. at a wavelength of 4.8 μm in the red curve of Fig. 4(d). This slight buckle that occurs in the simulation is not visible in the measurement and can be attributed to higher grating order. Different grating orders are present in the simulated spectra of the periodic antenna arrays, due to the collimated light in the simulations. They are sharper and located at slightly different spectral positions for the FDTD calculations compared to the angle-averaged FTIR microscope measurements [35]. In Fig. 4(d) and 4(e), e.g. the first grating order in respect to the silicon substrate occurs at around 4.8 μm and is visible as a slight buckle. In Fig. 4(f), the first grating order is shifted a bit more to the red due to the higher periodicity of this antenna array of 1.6 μm compared to 1.4 μm periods in 4(d) and 4(e). In the measurements, the presence of these grating orders is hardly visible due to the angle-averaging. Nevertheless, the spectral positions of the resonances as well as the overall lineshape can be reproduced satisfactorily by the FDTD simulations.

Our previous work showed the flexibility of this method, with which using a simple mask geometry one can produce a wide variety of possible antennae structures [24], especially if both proximity distance and exposure time are varied. This work concentrates mostly on the exposure time control without intentional changes to the proximity distance. Even in this case it was demonstrated that significant changes of size and form of the structures are easily realized. This allows fine-tuning of the resonance frequency within $\sim 20\%$ bandwidth. Moreover, the present work establishes robust transfer procedure from the relatively thin EUV exposed resist to metallic structures and demonstrates also for the first time IR resonance behavior of the antennae fabricated by this method. Together with a good agreement between experimental and simulation results, both for EUV mask diffraction and IR reflection calculation, this opens a way to fabrication of large-area arrays of structures with pre-programmed resonance properties.

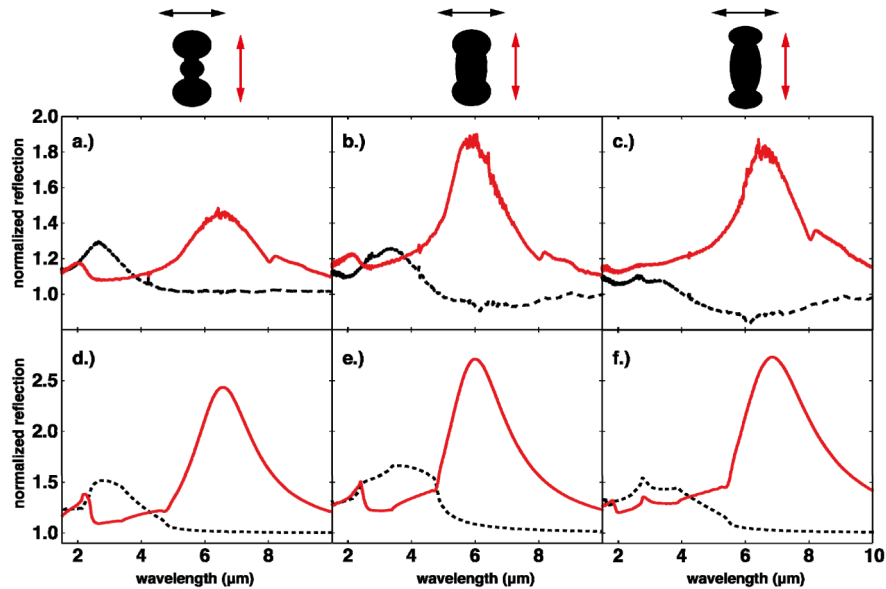


Fig. 4. Measured (a)-(c) and calculated (d)-(f) reflection spectra of the structures shown in Fig. 3 (d)-(f). The structure outlines are indicated above and the coloured arrows relate the spectra to the used polarisation directions. Red spectra correspond to a polarisation along the long axis and black dashed spectra to a polarisation along the short axis of the antennas, respectively.

4. Summary and outlook

We have demonstrated a new method for fast and flexible parallel fabrication of arrays of infrared antennas. Using a gas-discharge source and transmission masks with circular, triangular and rectangular aperture arrays, a bilayer stack of PMMA photoresists was illuminated with EUV radiation. Subsequent deposition of chromium and gold followed by a lift-off procedure resulted in arrays of nanoantennae with different shapes. Rectangular apertures on the mask result in a dumbbell-like shape of the antennas. Changes of exposure times and array periods result in significant variations of this geometry. FTIR reflection spectra of the antennas were obtained and compared to FDTD simulations demonstrating also a good agreement.

Future investigations will address the fabrication using various substrate materials in order to demonstrate an even higher flexibility of this fabrication method. As already described in [23], we plan to employ optical proximity correction techniques in order to enhance the resolution and improve our ability to design more complex antenna geometries. A direct etching method compared to the bilayer resist process could also significantly improve the homogeneity over large areas. Furthermore, with our ultra-short EUV wavelength we are not limited to fabrication of micrometer-sized antennas shown here. The presented method might also have a large impact on surface-enhanced spectroscopy when arrays of smaller structures will be realized to enable Surface Enhanced Raman Spectroscopy (SERS) [5].